A-4 SCIENTIFIC RESULTS

James Matteson
University of California, San Diego

In the previous paper, Dr. Levine discussed observations with the A-4 instrument below about 0.1 MeV. I would like to continue by discussing results that are for the most part at higher energies, from about 0.1 to 10 MeV, which could be called the low energy gamma-ray range or the extremely high energy X-ray range. Figure 1 shows that instrument layout. The detectors I am going to discuss are the high energy detector, located at the center of the instrument and collimated to 40 degrees full width at half maximum, and the four medium energy detectors located around the high energy detector and collimated to 16 degrees full width at half maximum. The high energy detector is designed to operate from about 0.5 to 10 MeV and the low energy detectors from about 0.05 to 2 MeV. Above about 0.2 MeV, the instrument is a first generation instrument, meaning that previous space instrumentation did not have the combination of sensitivity and angular resolution required to measure fluxes from point sources. Even in the low energy range of this instrument we could at best consider it a second generation instrument following in the paths of collimated scintillation counters flown on OSO-7 and OSO-8. Another point about the instrument I would like to make is that the requirements for extremely thick shielding to provide effective collimation above 1 MeV lead to the necessity to trade off sensitive area for shielding mass, with the result that the total instrument sensitive area is only about 500 cm^2 with about 300 cm^2 effective above 0.2 MeV. In Figure 2, I show the various fields of view that Dr. Levine showed earlier. This is to allow consideration of the instrument's ability to provide angular discrimination among the X-ray sources as we go from the highest energies, indicated by the large circle in Figure 2, to lowest energies, indicated by the crossed slats. The angular resolution improves as we go to lower energies. This allows reasonably unambiguous association of high energy flux discovered by this instrument with cataloged X-ray sources seen at low energies.

I would now like to discuss scientific results. I will not discuss the diffuse background. Our analysis of that is in work and within about a month, I think we will have something definitive to say. I also will not discuss gamma-ray pulsars and a large number of additional radio pulsars using HEAO pointings. This analysis is also in progress and results on Crab Vela pulsars should be available later this year. I will discuss some of the galactic sources, extra galactic sources, and finally, our observation of gamma bursts.

In Figure 3, I show some azimuthal scans. These are right shifted 90 degrees relative to what Dr. Levine showed you earlier and cover the 30 to 80 keV range. These data are from one of our medium energy

detectors which was intentionally operated at a slightly lower energy range to enhance the energy range overlap with the low energy detectors. The Crab Nebula and a complex of sources near the galactic center appear as strong sources. The wing to the left of the galactic center is GX 339-4 which you will recall from Dr. Levine's maps showed up as a resolved source approximately 20 degrees away from the galactic center. The fact that the low energy detectors show it is unconfused and that there are no other obvious hard X-ray sources within 10 degrees of it were used in deriving our medium energy spectrum of that source. Going to higher energies in Figure 4, I show the 79 to 150 keV range where the relative signature of the Crab Nebula and the galactic center is about the same. We also still see the wing on the left side of the galactic center due to GX 339-4. Extending up to 1 MeV in the lower part of the figure you can see a bump for the Crab Nebula and a statistically significant excess well above background for the galactic center region.

Now, I would like to discuss some of the objects associated with the azimuthal scan features in more detail. First, the Crab Nebula. Figure 5 is a spectrum of the Crab taken with medium energy detectors scanning data from a total of approximately 40 days in September 1977 and in March 1978. This is one of the most precise measurements of the spectrum of the Crab in this energy range, 25 keV to 1 MeV. Fifteen of the lower energy data points have statistical errors of only a few percent. Through extensive instrumental calibrations and Monte Carlo modeling, the systematic corrections of counts to photons also have accuracies of a few percent. The fitted spectrum has a power law index of 1.98 below 125 keV and 2.40 plus or minus about 0.1 above 125 keV. That is, we see a break in the spectrum at about 125 keV with a change in index of 0.4 ± 0.1. This is in reasonably good agreement with a recent NRL large area scintillation counter balloon observation which measured the break at slightly lower energy. That instrument was sensitive to only 180 keV, so its lever arm for establishing the higher energy spectrum was not particularly good. The dotted line in the figure is an extrapolation of the lower energy spectral fit. The large number of data points above 125 keV clearly lie well below the extrapolation. The upper limits are taken from our high energy detector data. These are 2σ upper limits and they also lie below the extrapolation. In Figure 6, I show a different representation of the same data. It is the data of the previous figure multiplied by energy squared. This has the convenience value of making an E^{-2} power law spectrum horizontal. The data from the observation I report here are indicated as dots. Below approximately 150 keV the error bars are usually too small to show. At higher energies the individual data points obtain statistical errors which are large enough to see. The break in the spectrum clearly occurs over a remarkably narrow energy band extending from only 100 to 200 keV. Above 200 keV the data are clearly falling well below the E^{-2} extension of the lower energy points. The break is just what is required to connect the high energy X-ray spectrum with the 100 MeV gamma-ray results of SAS-2 and COS-B. They see the Crab as

between 50 and 100 percent pulsed at high energies. The data I reported are the total emission of the Crab Nebula plus the central pulsar NP 0532. Here I take the observations of the pulsar by other workers, indicated by the dashed line, and subtract it from the total in order to obtain the spectrum of the nebula. You can see that this spectrum breaks at approximately 125 keV.

In Figure 7, I show the spectrum of the Crab Nebula from low frequency radio to extremely high energy gamma-rays. The break at about 10^{14} Hz is in the optical band. This break has long been taken as evidence for synchrotron radiation in the 3×10^{-4} gauss field of the Crab. It is the result of electron lifetime effects and the 1000 year age of the Nebula. In a 3×10^{-4} gauss magnetic field, an electron radiating at 125 keV would have a lifetime of only about 20 years. So, a short timescale acceleration process is required to maintain these electrons. From theoretical considerations, the Crab pulsar itself can only accelerate electrons to few times 10^{12} eV due to a curvature radiation cutoff. But to radiate at 125 keV requires another 50 times increase in the electron's energy. Theoreticians have speculated that this could be due to Fermi acceleration in the inner few tens of arc seconds of the Crab Nebula. In fact, lunar occultations observed in hard X-rays show that the Nebula is extended a few tens of arc seconds. So indeed these acceleration processes and the resulting energy spectrum of the electrons may be the origin of our observed break. Whatever its cause, the spectral break at 125 keV must be intimately related to acceleration and the loss processes in the central part of the Nebula.

Turning to the galactic center, in Figure 8 I show the spectrum we observed. The continuum radiation is indicated by the large dots. GX 339-4 is not included. The total luminosity of the galactic center in this energy band, 80 keV - 2 meV, is several times 10^{38} ergs per second. Thus far we have been unable to associate this emission with a single resolved low energy detector X-ray source. As Dr. Levine mentioned earlier, it appears that the emission is due to several sources within a few degrees of the galactic center. These sources apparently form a new class of X-ray emitters with high energy X-ray luminosities up to approximately 10^{38} ergs per second, ranking them among the most luminous point-like X-ray sources known. We have also searched for nuclear gamma-rays from the galactic center and have not been successful. In Figure 9, the gaussian shown at 4.4 MeV is our predicted response to a 10^{-3} photon/cm^2-sec flux. Gamma-rays at this energy are expected due to cosmic ray excitation of the interstellar medium and in fact, the Rice group reported an observation at about 3σ significance at that flux level from the galactic center. We had hoped to confirm it; in fact, our 3σ upper limits are 3.7×10^{-4} for a narrow line and 5×10^{-4} for a broader line. We conclude that either the line is significantly below the level reported by Rice or it is transient.

We performed a pointed observation of Cygnus X-1 on several occasions since it is one of the most interesting X-ray sources. Figure 10, adapted from a review by Oda, shows the geometry of the Cygnus X-1 X-ray source. A hot torus with dimension approximately 100 km surrounds the black hole and emits X-rays. Accidently, we were once in a mode which did not give us the high time resolution we wanted, but instead gave us a good spectral resolution (Fig. 11). This was fortunate because during normal scanning there is insufficient time once a source occurs to obtain precision spectra at high energies. Notice the extremely small error bars and obvious departures from a simple power law spectrum. The spectrum steepens above 60 to 70 keV as is characteristic of Cygnus X-1. Theoreticians thinking about X-ray emission processes in Cygnus X-1 and other objects will be able to use this and similar spectra of other sources to perform detailed model testing. Figure 12 shows 160 msec timing data taken in two energy bands. The lower trace is the 14 to 32 keV band, middle is the 32 to 160 keV band, and the upper is their sum. We see flares from Cygnus X-1 occurring in both energy bands simultaneously. Intensity dips also occur. This is the first time it has been possible to do the type of high time-resolution observation required to extend shot noise and correlation analysis to energies above 20 keV. I would like to point out that about 70 percent of the power from Cygnus X-1 is radiated above 20 keV, so any theoretical understanding of the processes in this object must be biased by observations at these energies. Figure 13 shows spectra taken by randomly picking up high, low, and averaged intensity states. You see that the spectrum of Cygnus X-1 does not appear to change shape significantly over about a factor of six in intensity. Figure 14 is a more detailed analysis, showing the spectral hardness ratio over a larger range of intensity units. Below 5 units we see a slight indication of spectral softening. Here intensity is very near to background and nearly zero, so there may be a systematic effect in the data analysis.

Refer to Figure 15. We performed autocorrelations on the two energy bands and the total. They all show essentially the same form; a steep drop and then a tail. For times less than 1 sec they appear similar to previous results. The tail extending out to a few tens of seconds is new. Figure 16 shows the 14-160 keV autocorrelation in detail. Below a half second it is fitted by an exponential with approximately 0.7 sec time constant, as is often seen in 2 to 20 keV analysis of other observations. The 2.2 sec component is required to fit the data at larger times. It is persistent in 5 observations and subsets of them.

Figure 17 shows the cross correlation between low and high energy and here is where some important physics comes in. The point is to determine whether high energy X-rays lead or lag the low energy X-rays. A definite measurement of such an effect would have significant theoretical implications for the processes in the inner accretion disc. The eye says there is no obvious trend here, and an analysis by Pat Nolan, a graduate student at San Diego, shows that to about 10 msec accuracy there is no lag. What does this mean for Cygnus X-1? I think that these results

are consistent with the concept of Compton cooling which was proposed several years ago as the X-ray generation process in the inner accretion disk. Here you have 10^9 K electrons being cooled by Compton scattering of soft photons. High energy X-rays result. The fact that the spectrum does not change with intensity indicates that geometry of the scattering region is probably independent of the luminosity. The X-ray intensity fluctuations are possibly due to fluctuations in the soft flux which is the source of the photons which ultimately cool Cygnus X-1.

Figure 18 shows GX 339-04 which has been discussed several times earlier today as a black hole candidate due to its similarity to Cygnus X-1. The short time scale variability in two state spectrum exhibited by this object are also characteristics of Cygnus X-1. The new result we have here is an extension of its spectrum up to several hundred keV. For reference I have shown the spectrum of Cygnus X-1. They are each quite hard and have a steepening above approximately 100 keV. This is additional evidence for the similarity between these two objects. In addition, the intensity of GX 339-04 is a factor of 4 or 5 below Cygnus X-1, consistent with the estimated distances to these objects.

I next turn to extra-galactic objects. Centaurus A is the only extra-galactic object which is clearly visible in Dr. Levine's sky maps in the first 6 months of the mission. Our medium energy detector data for this object, the small dots in Figure 19, extend the spectrum up to about 700 keV, confirming the Rice balloon observation of high energy X-ray emission in this object. Since the spectrum is quite hard, about $E^{-1.6}$ in our observation, the X-ray luminosity of Centaurus A is dominated by the highest energy where significant X-ray emission is occurring. The data which I just discussed were taken in January of 1978. In July-August 1978, we observed again. The large dots are the results. We do not have any low energy data available yet, so these are only medium energy detector results. A factor of 2 intensity decrease occurred over the 6 months and the spectrum shape stayed roughly constant, although we cannot say much about it. Centaurus A is known to have temporal and spectral variabilities in X-rays on time scales of a few years. We have now reduced that time scale to 6 months.

Turning to 3C273 (Fig. 20) I show on the right panel the data taken during the "ping-pong" pointing observations that lead to the spectrum which Dr. Boldt showed earlier, the A-2 spectrum extending from a few keV up to about 60 keV. Also on the right panel, the A-4 results are seen as the four data points from 13 to 125 keV. The motivation for the observation was that COS-B had reported a gamma X-ray flux from 3C273 at 100 Mev. Therefore, it was a good candidate for detectable X-ray emission above 100 keV. But the flux was expected to be very low, so a long duration "ping-pong" observation was spread over three periods. It paid off. The $E^{-2.05}$ power law is capable of connecting the A-4 and COS-B results, although A-4 fitted strictly by

itself leads to a harder spectrum, $E^{-1.7}$. Figure 21 is the same figure which Dr. Boldt presented earlier. The crosses below 60 keV are from A-2, the diamonds are A-4 low energy detector points and the cross from 100 to 300 keV is an A-4 medium energy detector datum from scanning observations.

Referring to Figure 22, I would like to discuss two gamma-ray bursts. We have analyzed a few gamma-ray bursts. I am sure that there are many in the data. An important new observation that we have provided is the measurement of the spectrum on short time scales at high energies. For comparison purposes, the Apollo 16 burst is shown. The October 20, 1977, burst was temporal structure similar to the Apollo 16 burst except that it has a couple of peaks occurring after the main burst. These are numbered 3 and 4 and occur on approximately 10 sec centers. This may be an indication of periodicity. Also shown in Figure 22 is the November 10, 1977 burst which had only one peak, number 5. I have numbered the peaks 1 through 5. Their spectra are shown in Figure 23. For reference, the solid line is the Apollo 15 spectrum. It is not too obvious to those of you in the back of the room, but if we disregard the lowest energy point which we were having some problems with, each of these five spectra are essentially identical. They are varying in intensity but not in shape or effective temperature. From that we conclude that the intensity variations are a property of the energy source, or reservoir, for the gamma-ray burst, perhaps accretion onto some compact object and that the spectrum shape is a signature of the physics of the engine that powers these objects, perhaps the potential well into which the matter may be falling.

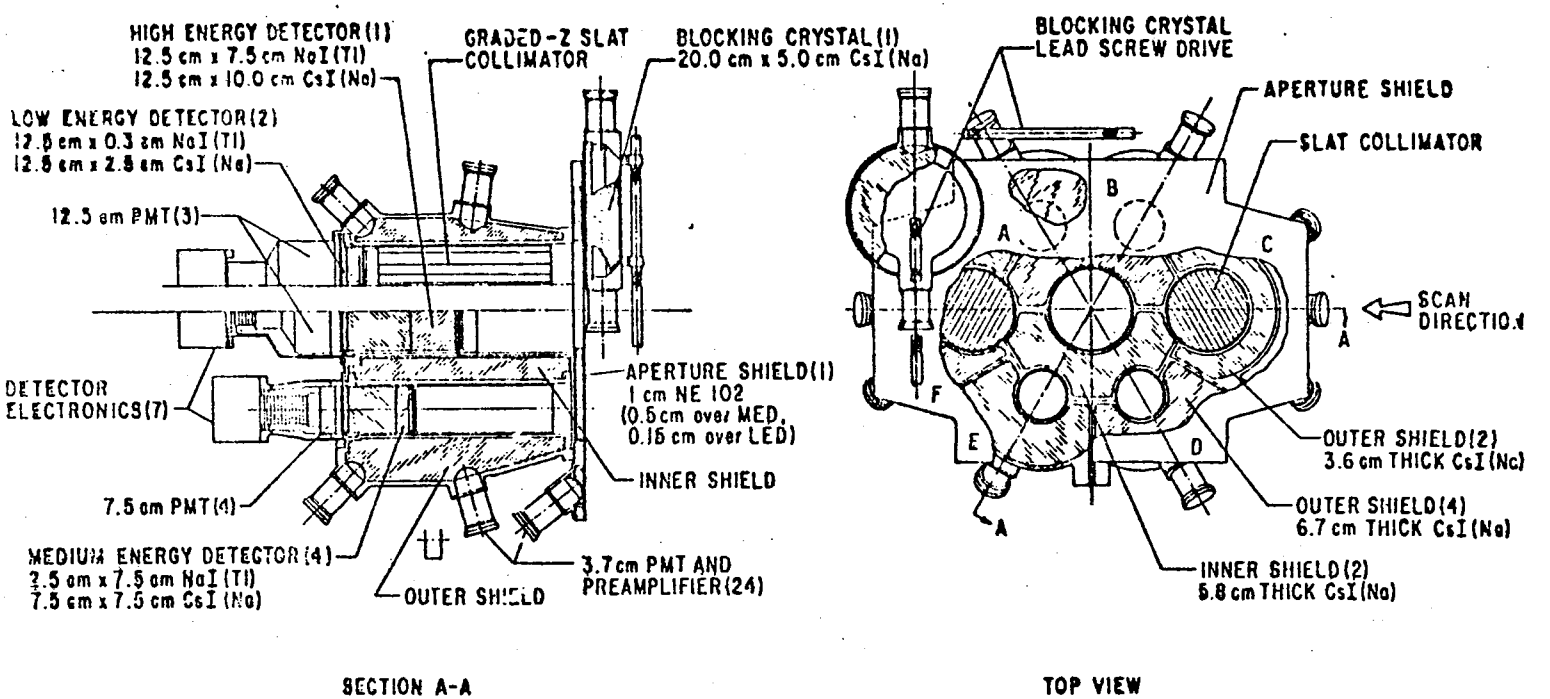

UCSD, MIT HARD X-RAY AND LOW ENERGY GAMMA-RAY
INSTRUMENT OF HEAO-1

Figure 1

HEAO A-4

FULL WIDTH FIELDS OF VIEW

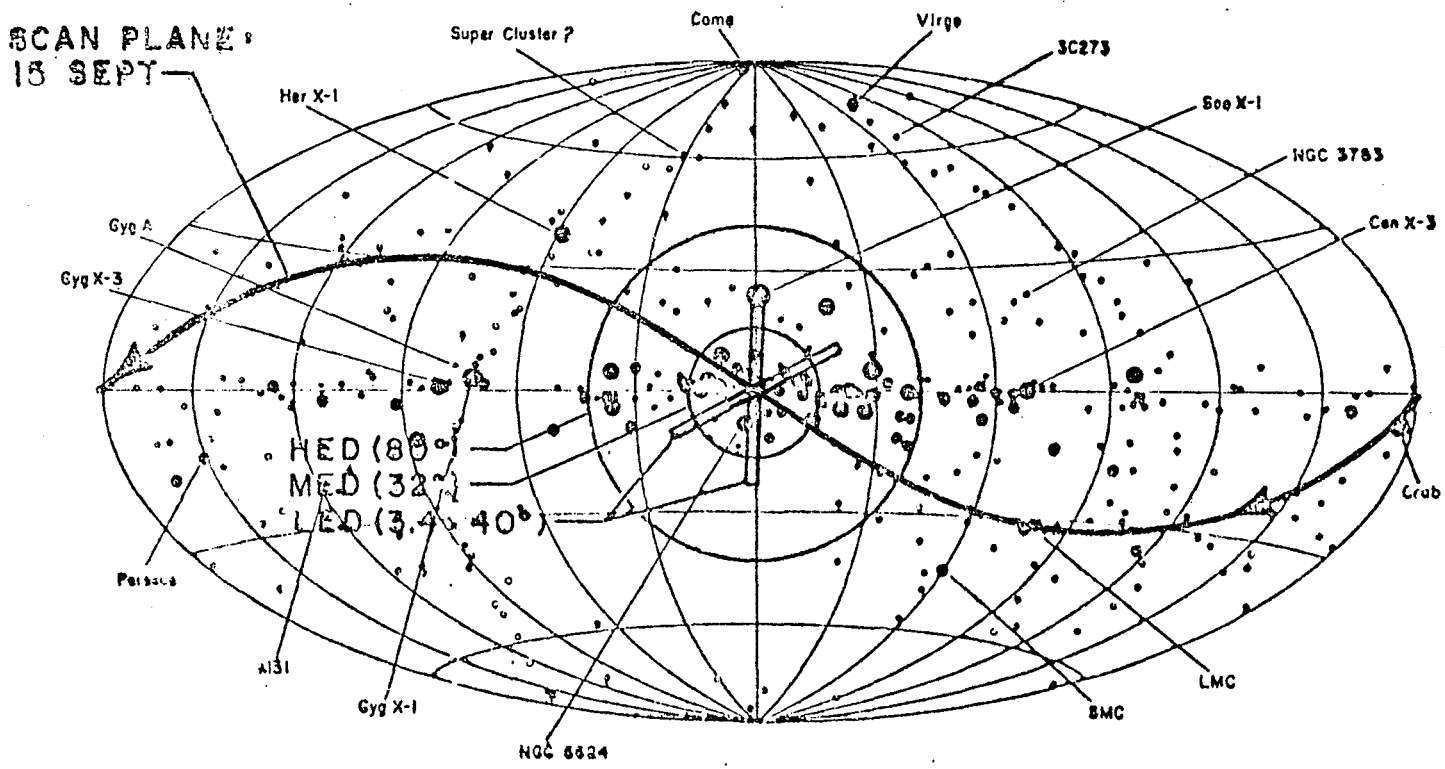

Figure 2

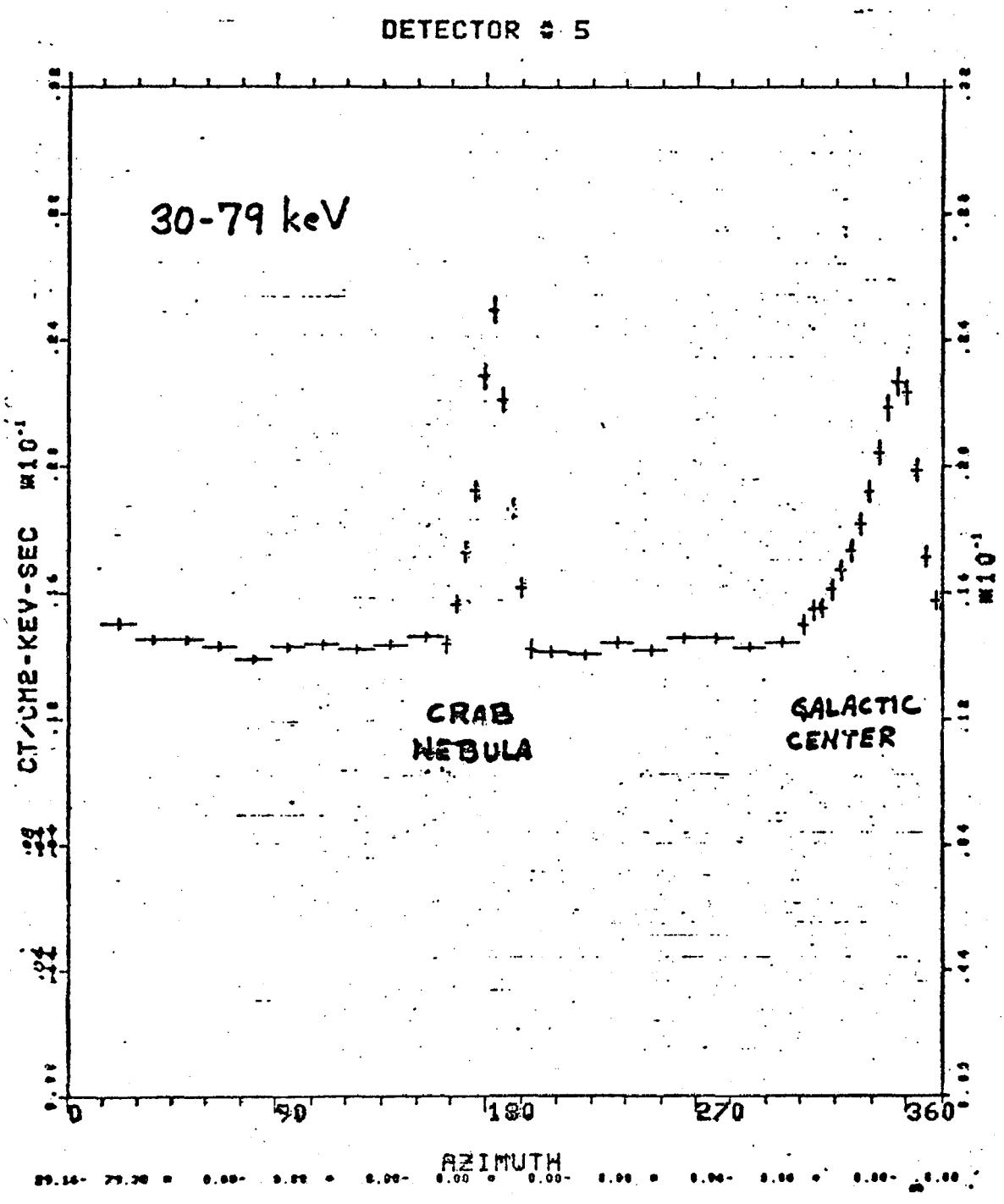
DETECTOR # 5
30-79 keV
CRAB NEBULA
GALACTIC CENTER
CT/CM2-KEV-SEC
0
90
180
270
360
AZIMUTH

Figure 3

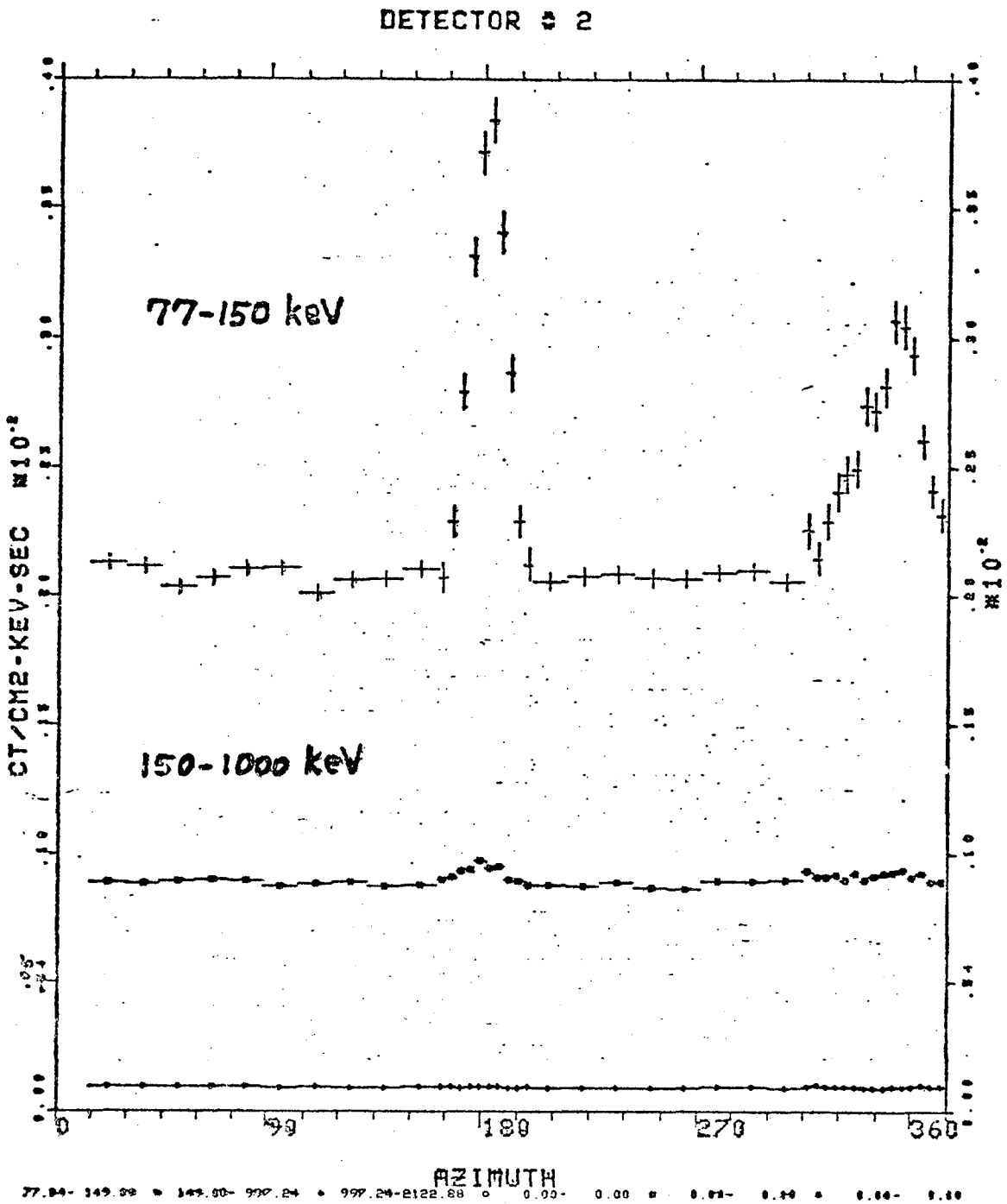
DETECTOR # 2
77-150 keV
150-1000 keV
CT/CM2-KEV-SEC
0
90
180
270
360
AZIMUTH

Figure 4

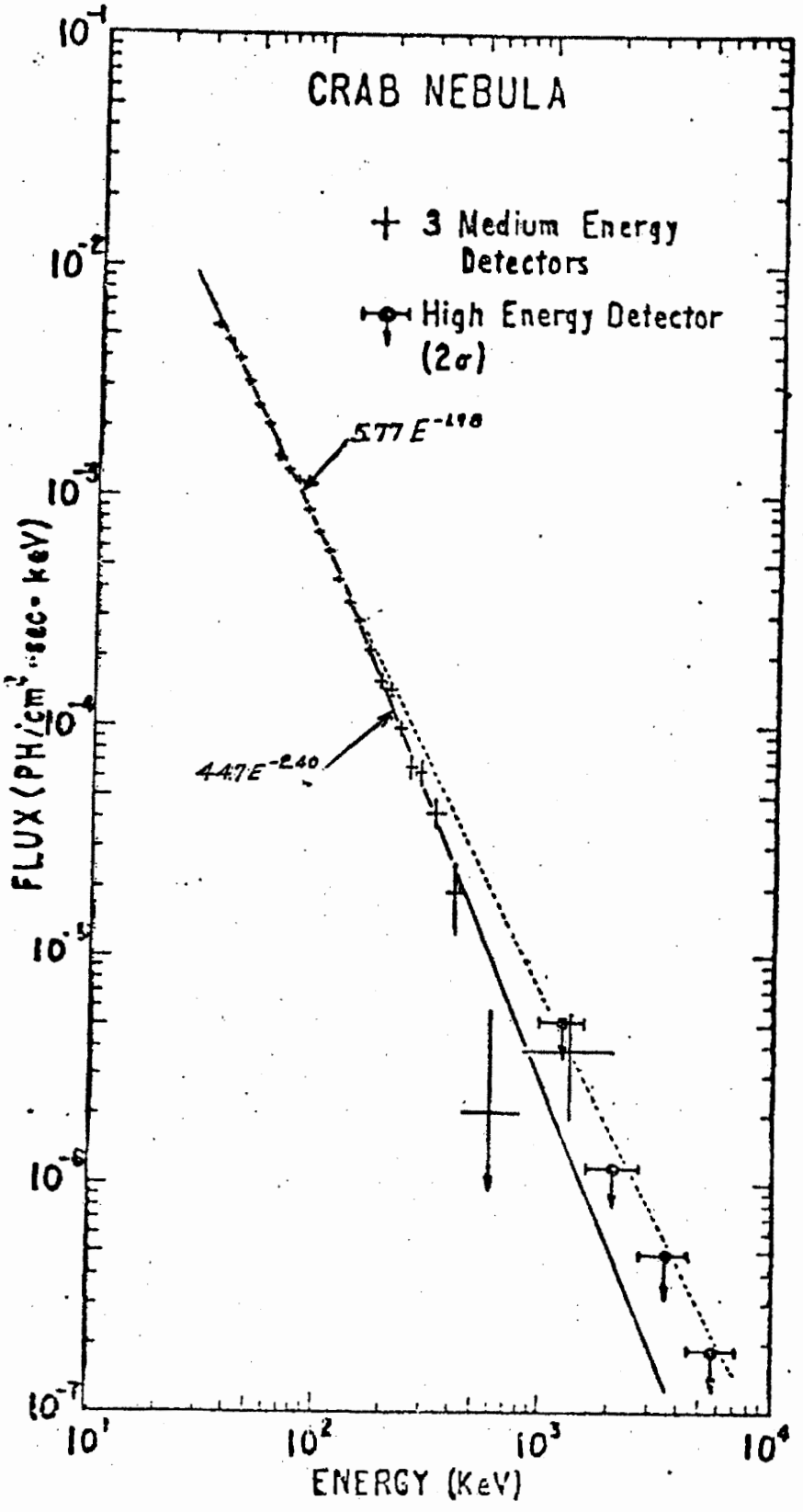
CRAB NEBULA
3 Medium Energy Detectors
High Energy Detector (2σ)
5.77 E^-1.18
4.47E^-2.40
FLUX (PH/cm²·sec·keV)
ENERGY (KeV)
10^-1
10^-2
10^-3
10^-4
10^-5
10^-6
10^-7
10^1
10^2
10^3
10^4

Figure 5

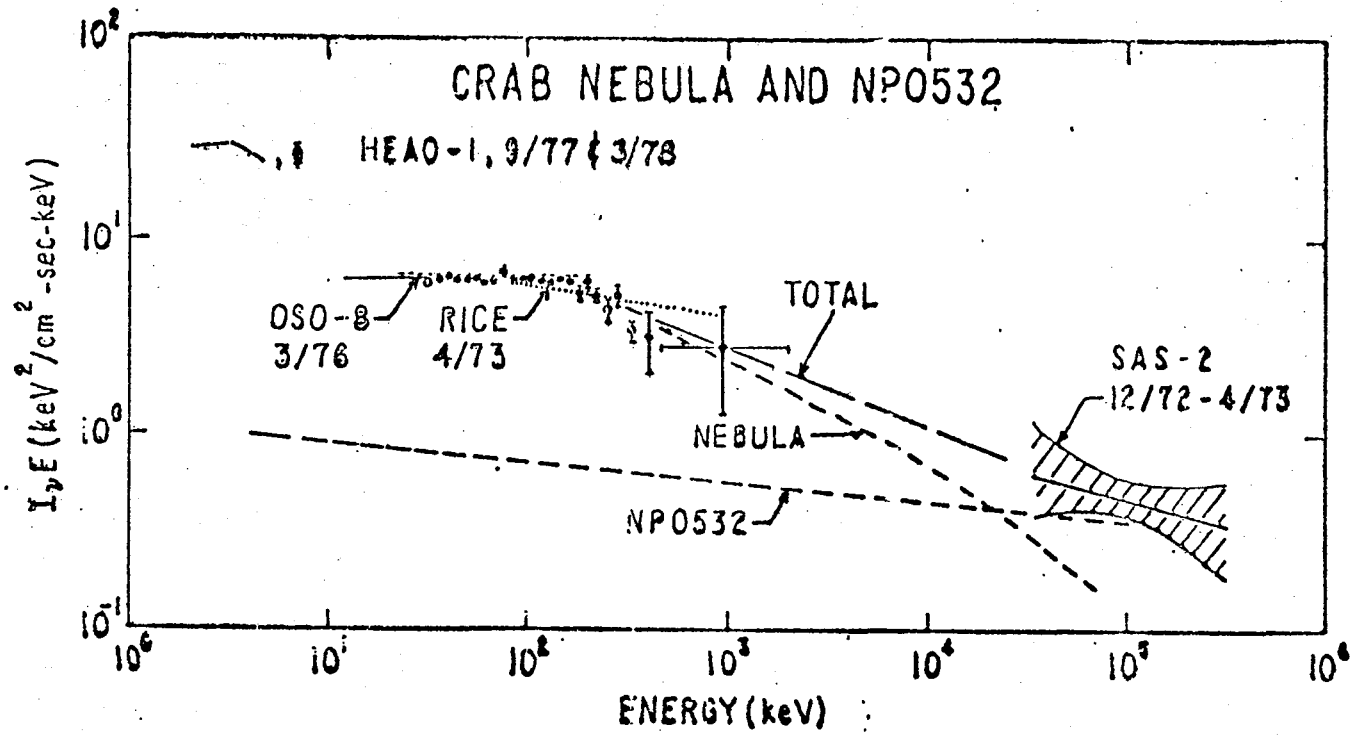
CRAB NEBULA AND NP0532
HEAO-1, 9/77 & 3/78
OSO-8
3/76
RICE
4/73
TOTAL
NEBULA
NP0532
SAS-2
12/72-4/73
$I_\nu E$ (keV^2/cm^2-sec-keV)
ENERGY (keV)

Figure 6

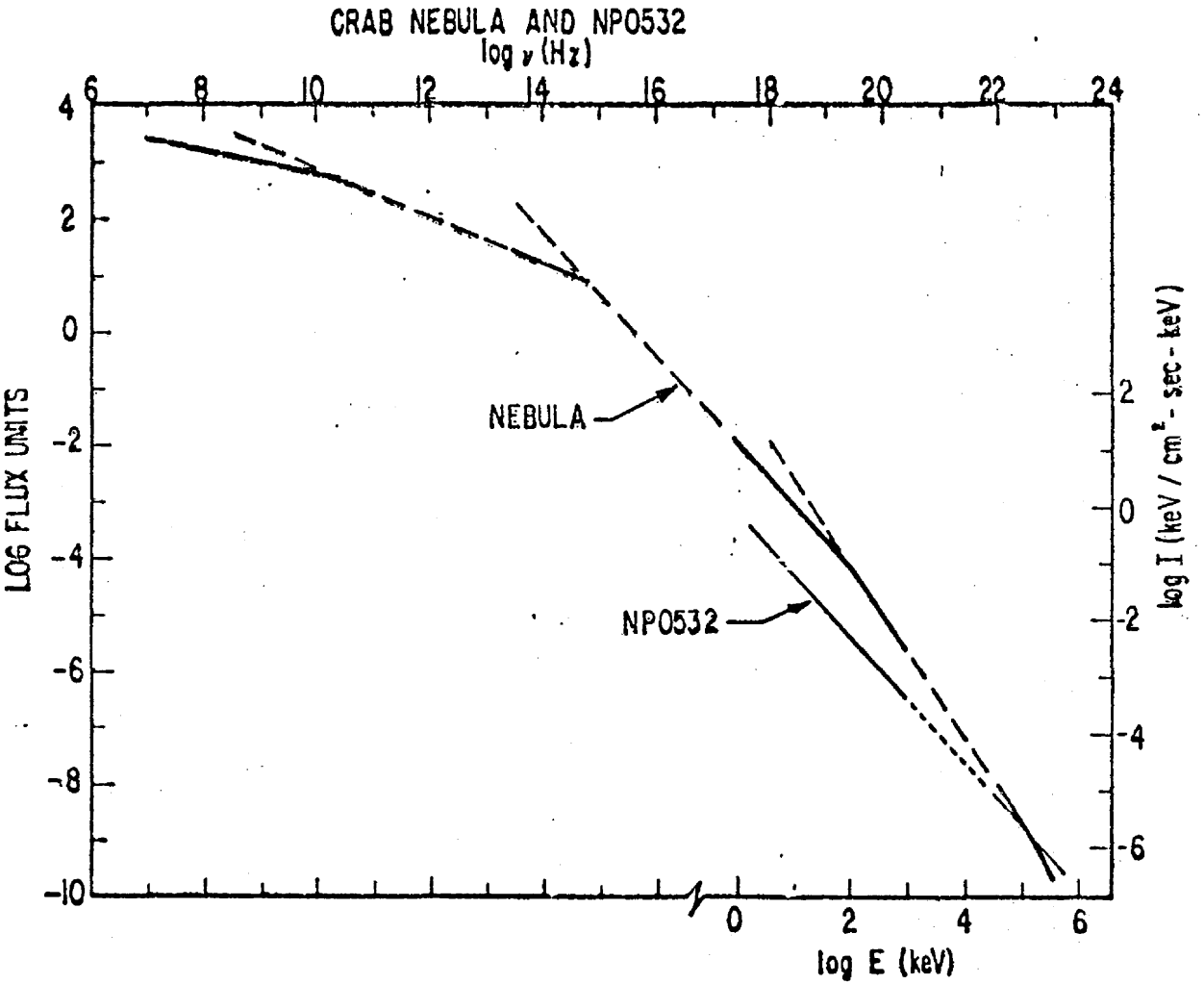
CRAB NEBULA AND NP0532
log ν (Hz)
6
8
10
12
14
16
18
20
22
24
4
2
0
-2
-4
-6
-8
-10
LOG FLUX UNITS
NEBULA
NP0532
0
2
4
6
log E (keV)
2
0
-2
-4
-6
log I (keV / cm² - sec - keV)

Figure 7

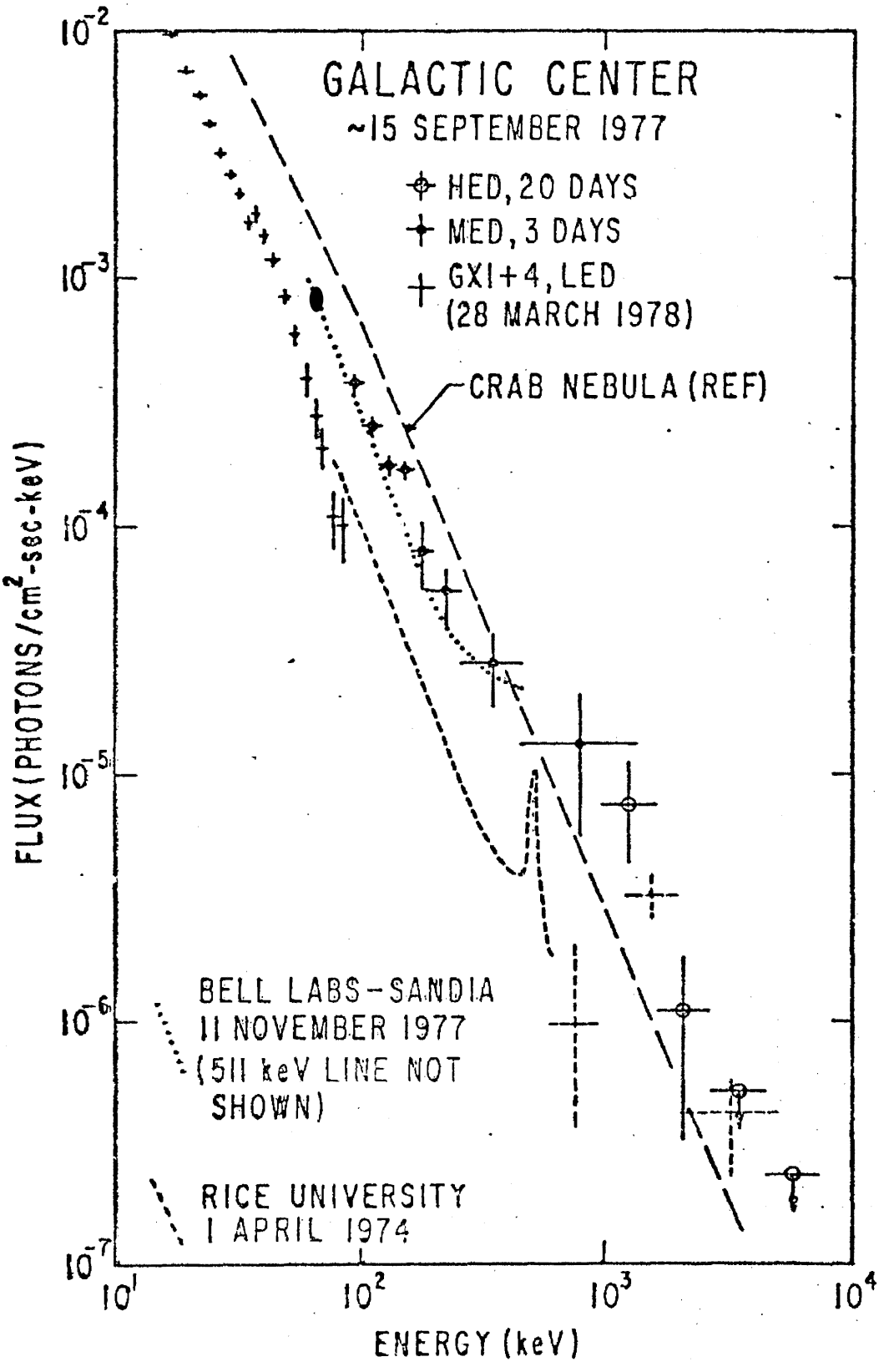
GALACTIC CENTER
~15 SEPTEMBER 1977
HED, 20 DAYS
MED, 3 DAYS
GXI+4, LED
(28 MARCH 1978)
CRAB NEBULA (REF)
BELL LABS-SANDIA
11 NOVEMBER 1977
(511 keV LINE NOT
SHOWN)
RICE UNIVERSITY
1 APRIL 1974
FLUX (PHOTONS/cm²-sec-keV)
ENERGY (keV)
10⁻²
10⁻³
10⁻⁴
10⁻⁵
10⁻⁶
10⁻⁷
10¹
10²
10³
10⁴

Figure 8

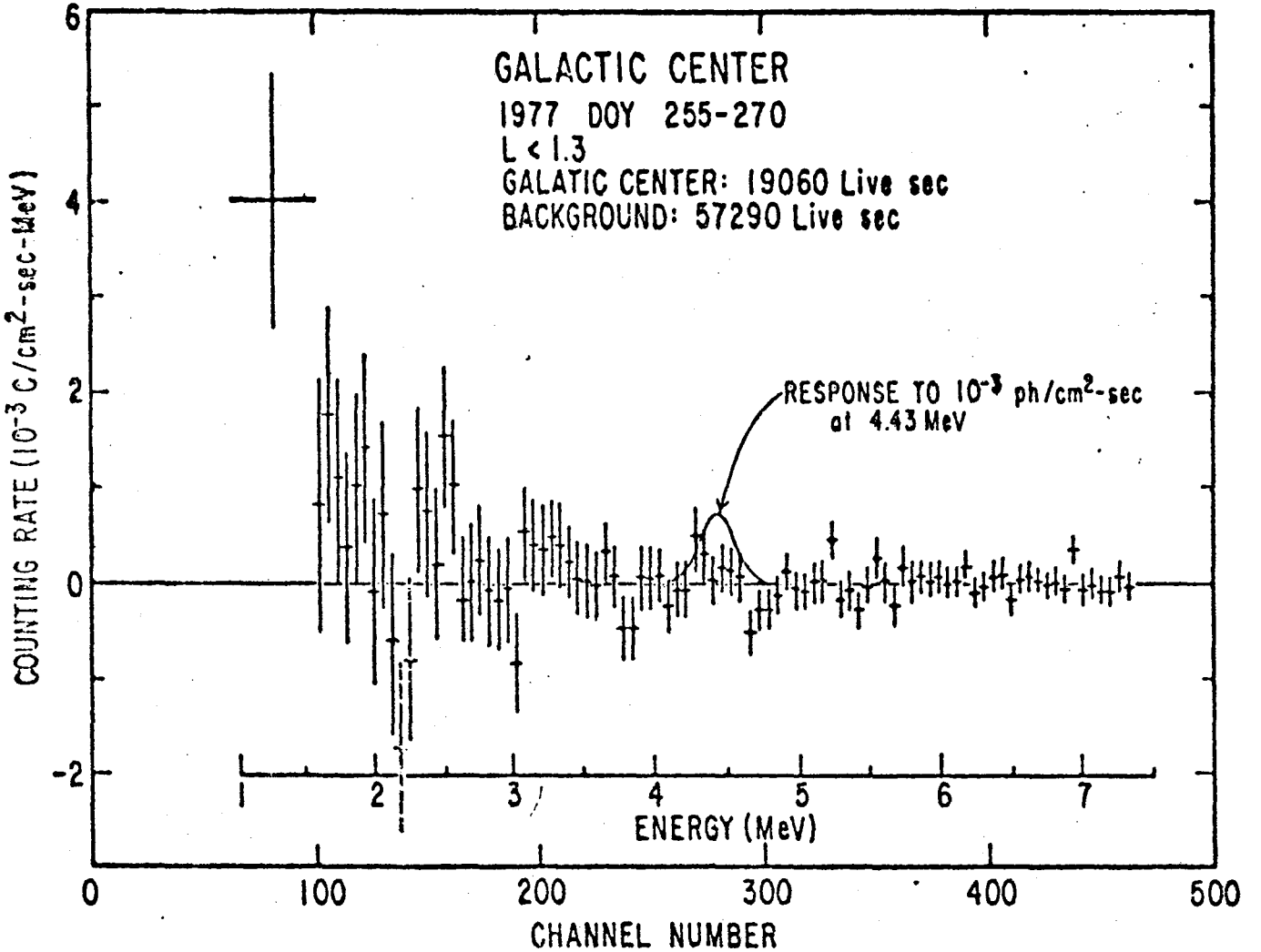
GALACTIC CENTER
1977 DOY 255-270
L < 1.3
GALATIC CENTER: 19060 Live sec
BACKGROUND: 57290 Live sec
RESPONSE TO 10⁻³ ph/cm²-sec at 4.43 MeV
COUNTING RATE (10⁻³ C/cm²-sec-MeV)
6
4
2
0
-2
1
2
3
4
5
6
7
ENERGY (MeV)
0
100
200
300
400
500
CHANNEL NUMBER

Figure 9

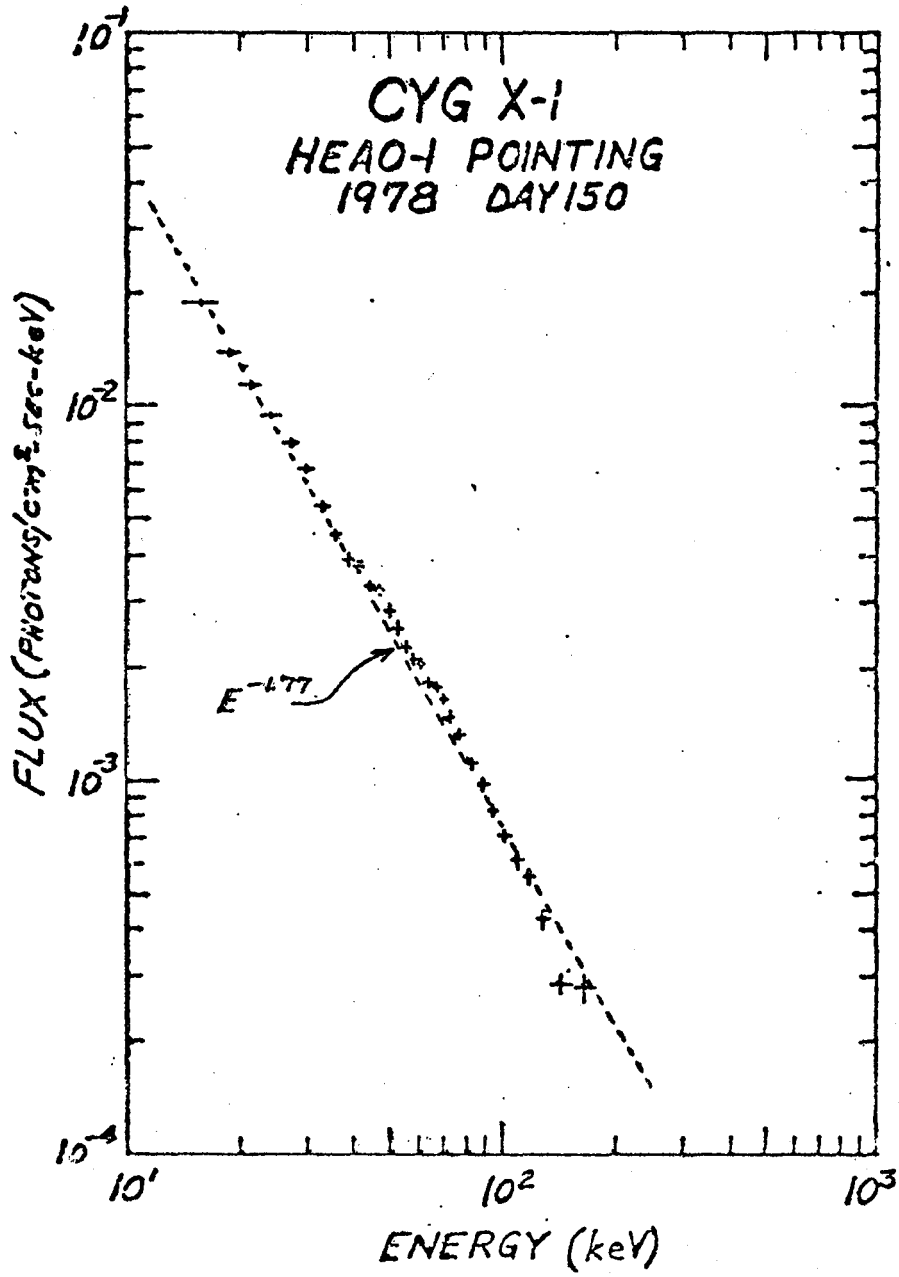
CYG X-1
HEAO-1 POINTING
1978 DAY 150
FLUX (PHOTONS/CM²-SEC-keV)
10^{-1}
10^{-2}
10^{-3}
10^{-4}
$E^{-1.77}$
10^{1}
10^{2}
10^{3}
ENERGY (keV)

Figure 10

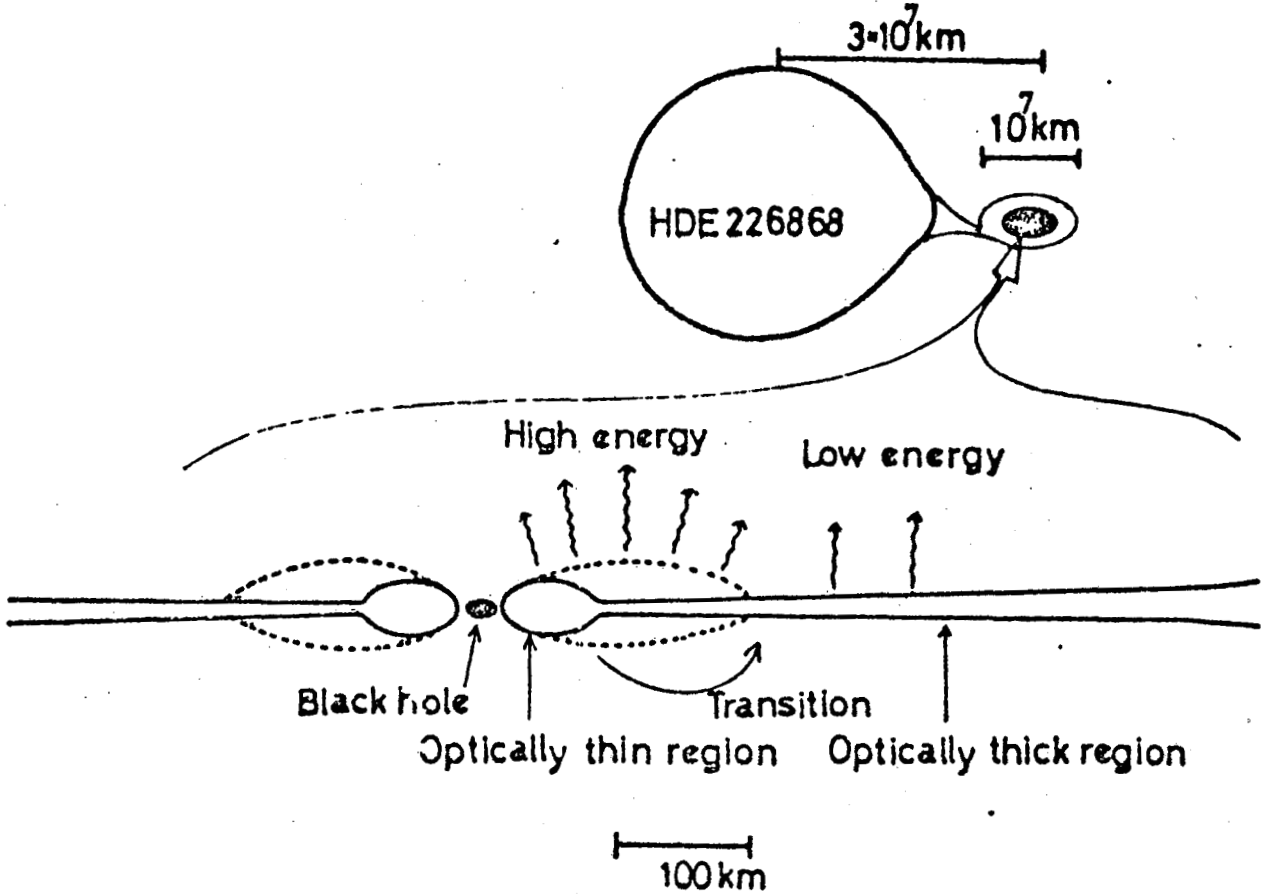
3·10^7km
10^7km
HDE 226868
High energy
Low energy
Black hole
Transition
Optically thin region
Optically thick region
100km

Figure 11

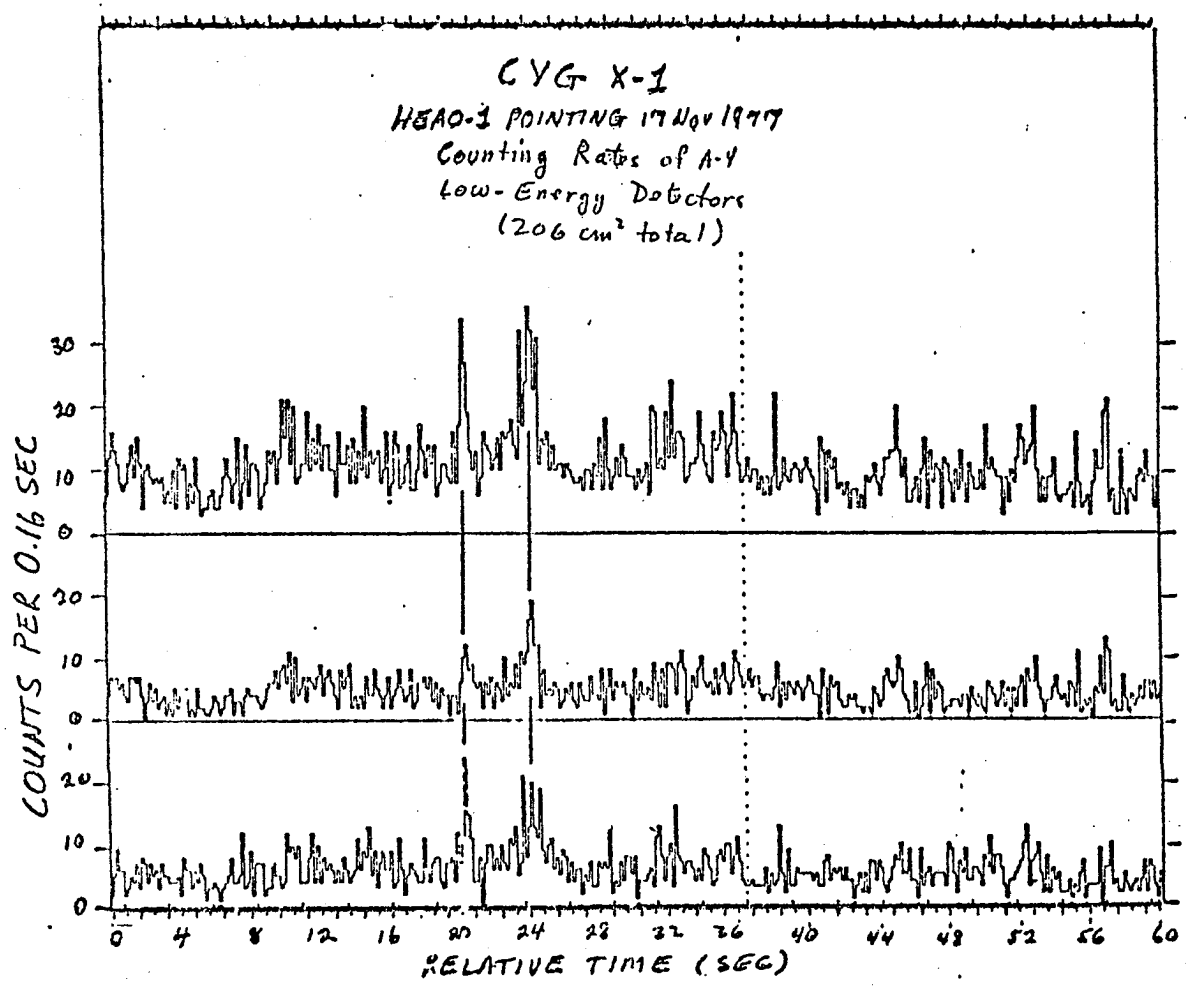
CYG X-1
HEAO-1 POINTING 17 Nov 1977
Counting Rates of A-4
Low-Energy Detectors
(206 cm² total)
COUNTS PER 0.16 SEC
30
20
10
0
20
10
0
20
10
0
0
4
8
12
16
20
24
28
32
36
40
44
48
52
56
60
RELATIVE TIME (SEC)

Figure 12

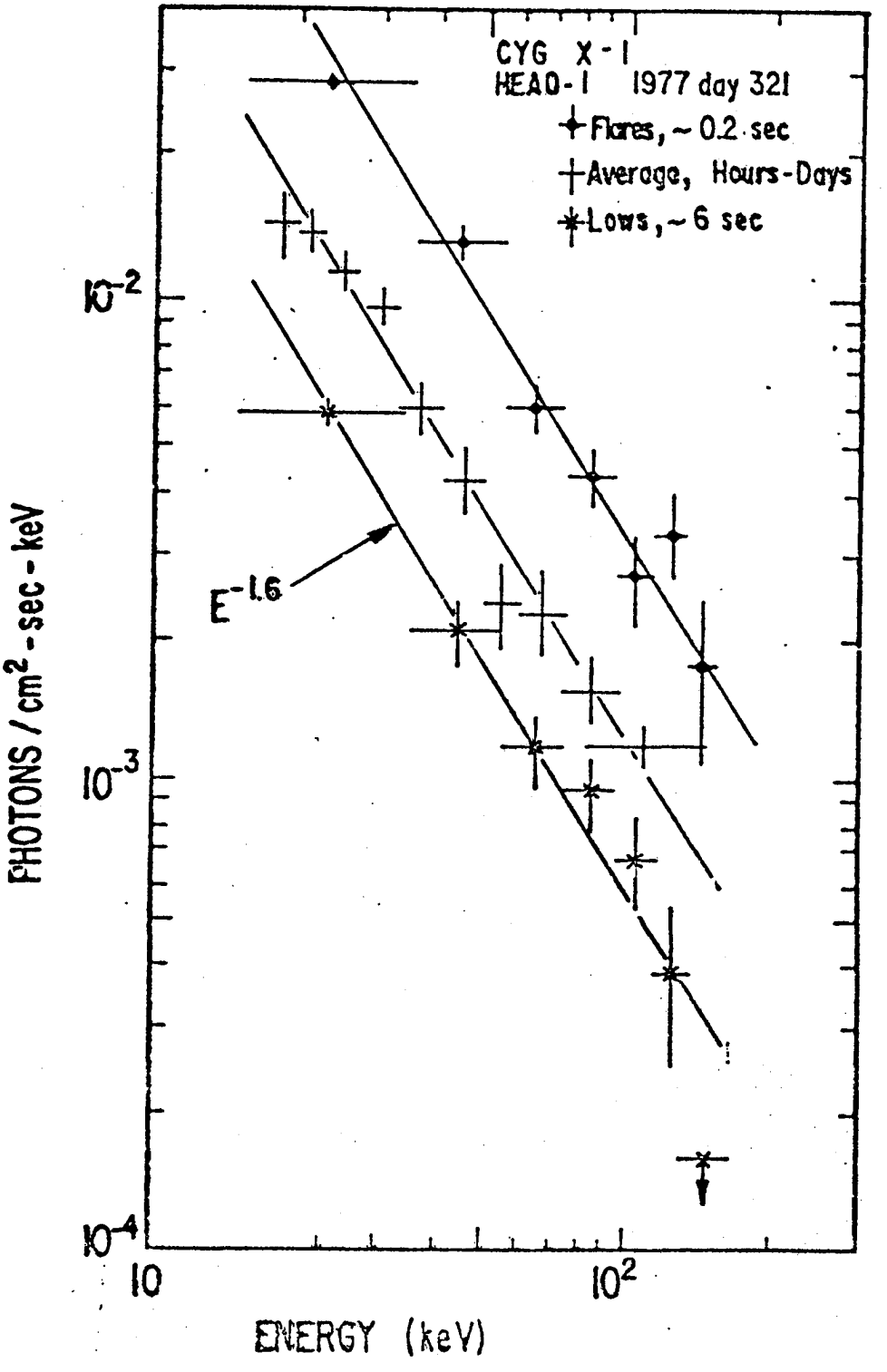
CYG X-1
HEAO-1 1977 day 321
Flares, ~ 0.2 sec
Average, Hours-Days
Lows, ~ 6 sec
10^{-2}
10^{-3}
10^{-4}
$E^{-1.6}$
PHOTONS / cm^2 - sec - keV
10
10^2
ENERGY (keV)

Figure 13

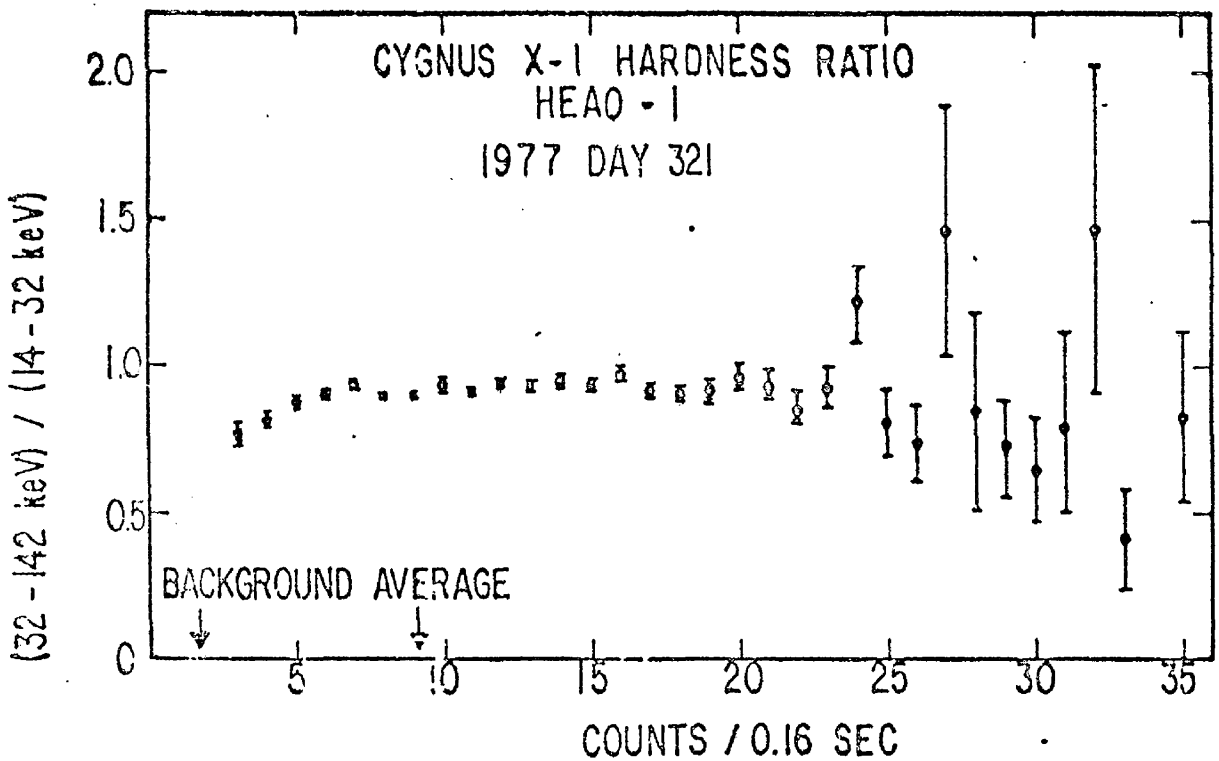
CYGNUS X-1 HARDNESS RATIO
HEAO - 1
1977 DAY 321
(32 - 142 keV) / (14 - 32 keV)
2.0
1.5
1.0
0.5
0
BACKGROUND AVERAGE
5
10
15
20
25
30
35
COUNTS / 0.16 SEC

Figure 14

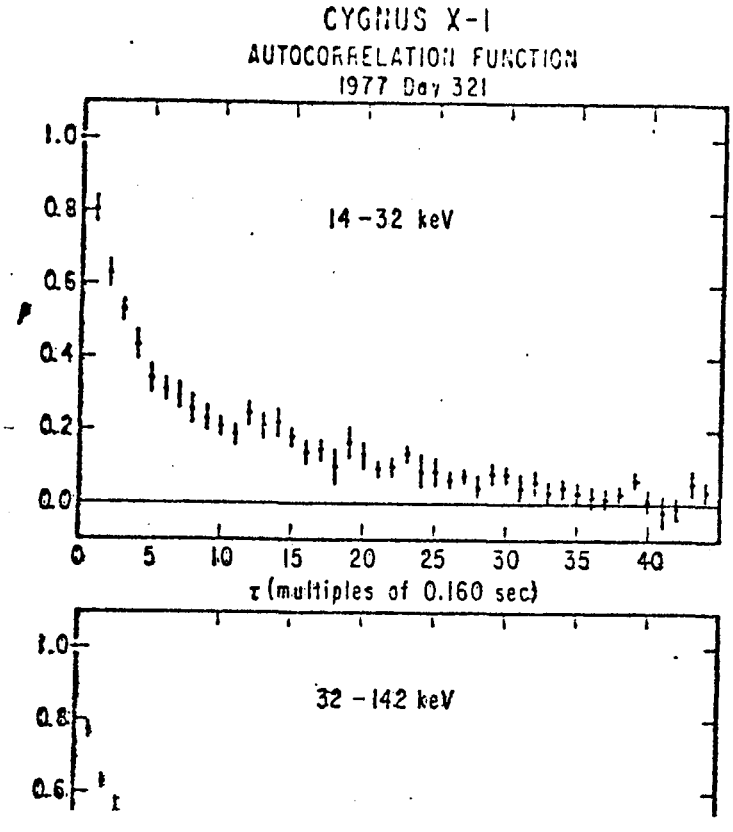
CYGNUS X-1
AUTOCORRELATION FUNCTION
1977 Day 321
14 - 32 keV
1.0
0.8
0.6
0.4
0.2
0.0
P
0
5
10
15
20
25
30
35
40
τ (multiples of 0.160 sec)
32 - 142 keV
1.0
0.8
0.6

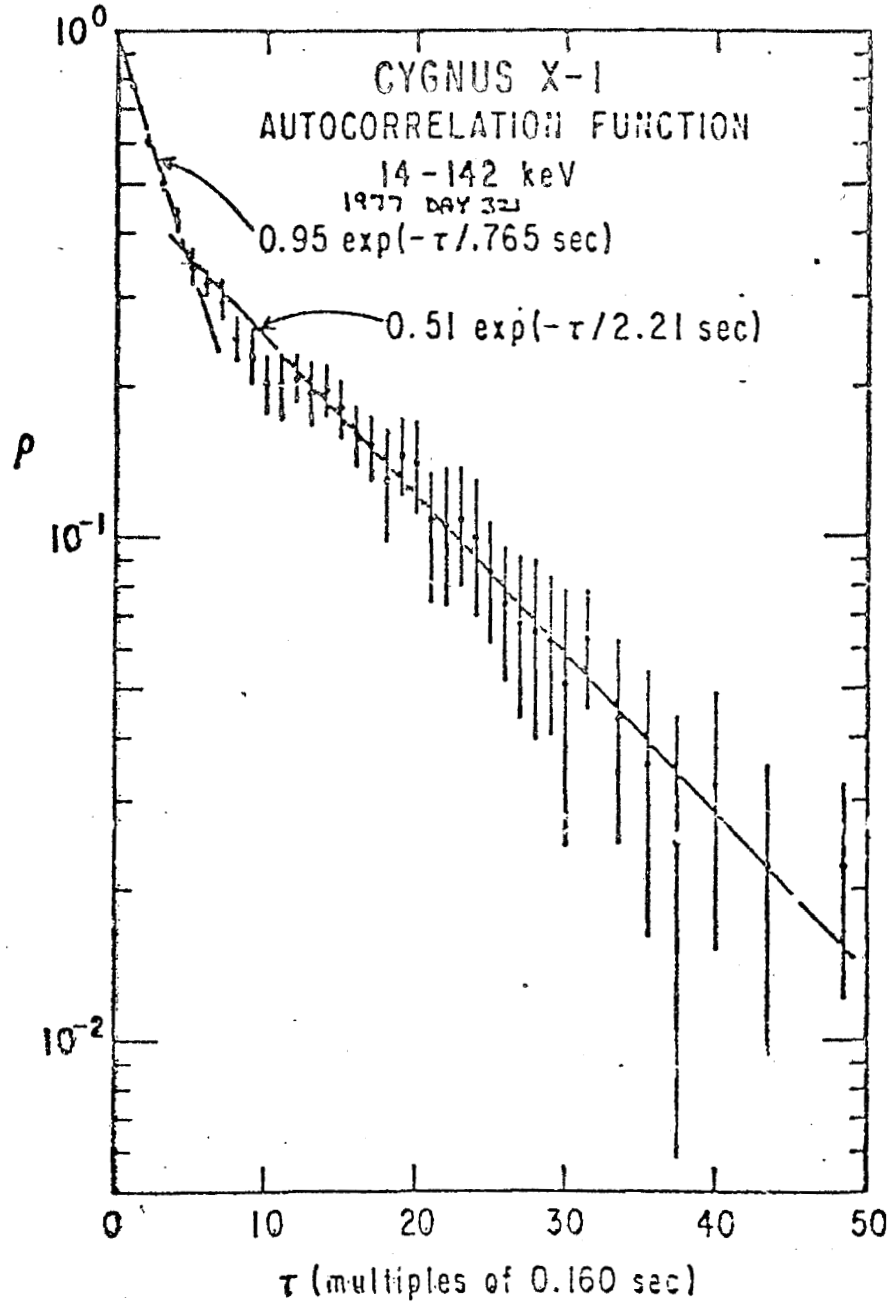
CYGNUS X-1
AUTOCORRELATION FUNCTION
14 - 142 keV
1977 DAY 321
0.95 exp(-τ/.765 sec)
0.51 exp(-τ/2.21 sec)
ρ
10^0
10^-1
10^-2
0
10
20
30
40
50
τ (multiples of 0.160 sec)

Figure 16

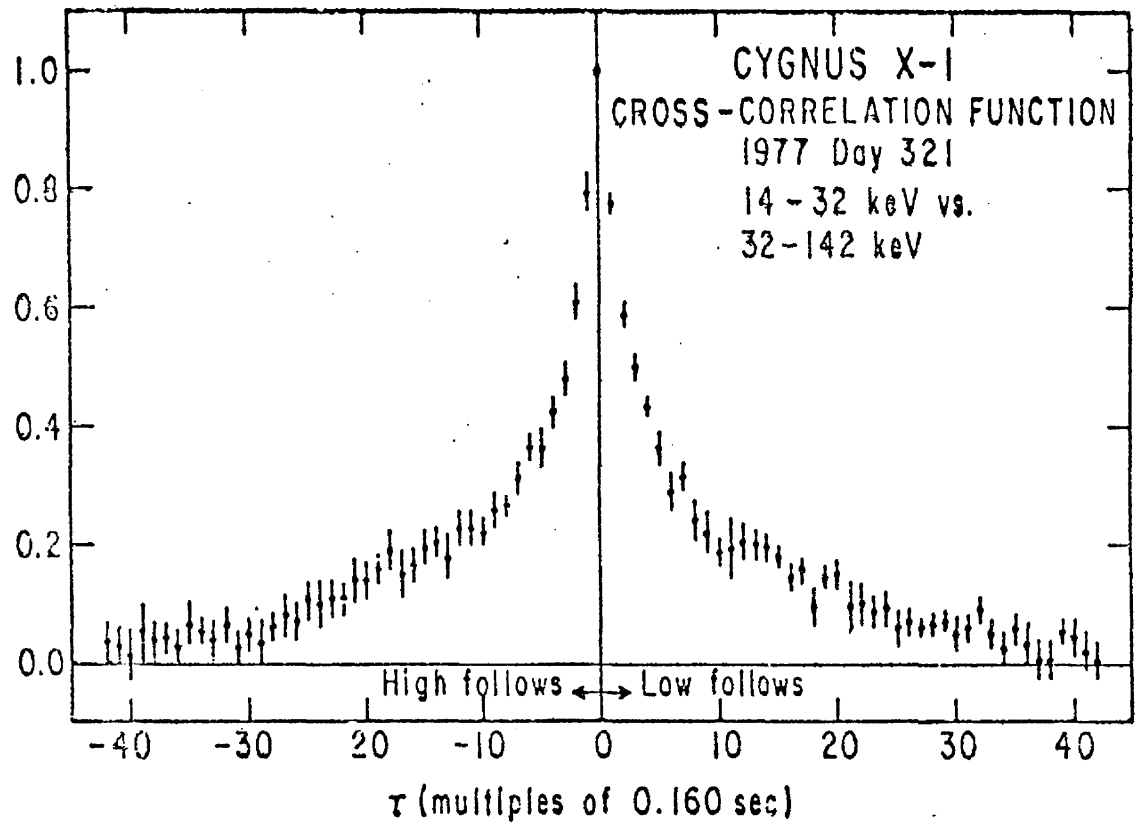
CYGNUS X-1
CROSS-CORRELATION FUNCTION
1977 Day 321
14 - 32 keV vs.
32 - 142 keV
1.0
0.8
0.6
0.4
0.2
0.0
High follows
Low follows
-40
-30
20
-10
0
10
20
30
40
τ (multiples of 0.160 sec)

Figure 17

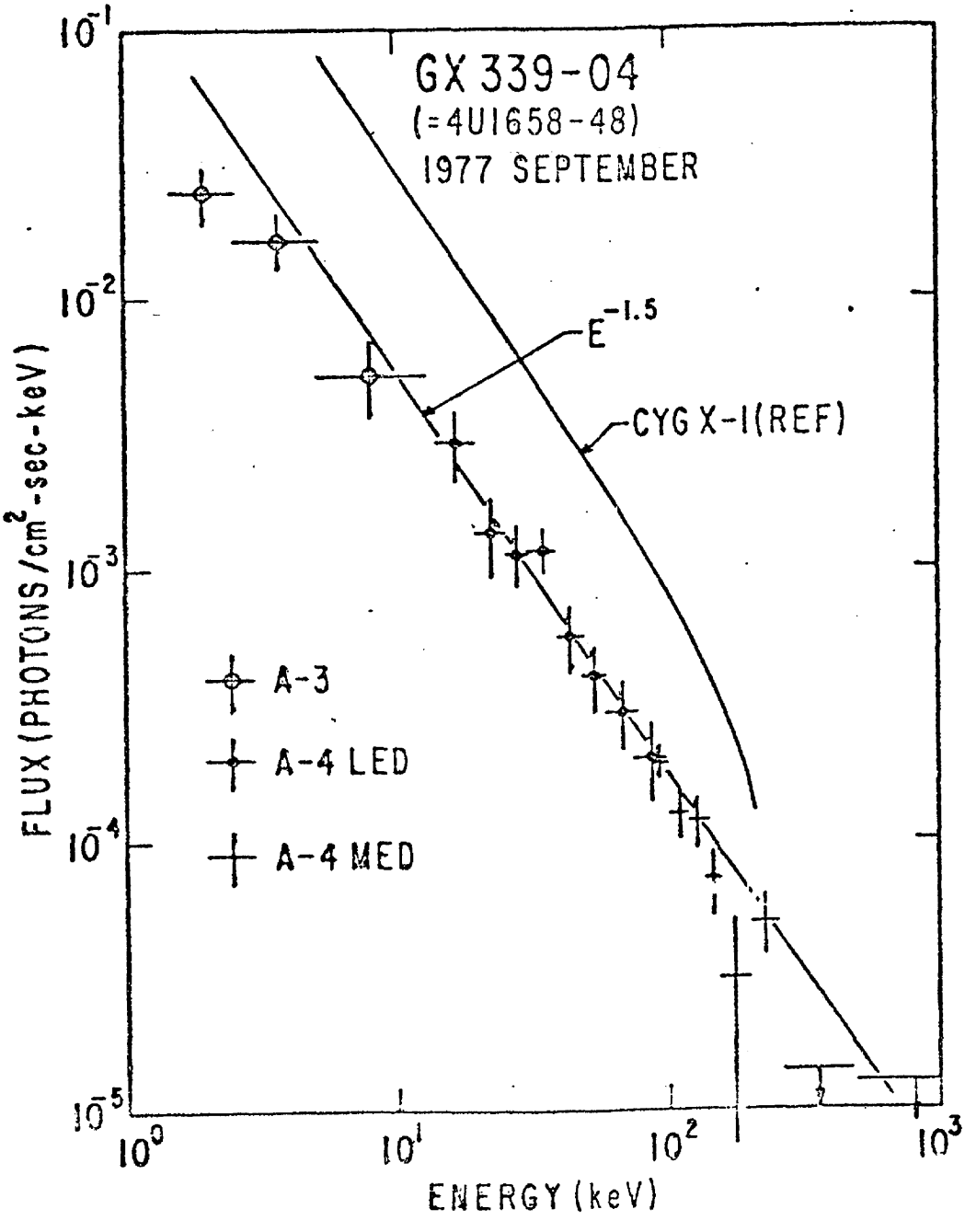
GX 339-04
(=4U1658-48)
1977 SEPTEMBER
$E^{-1.5}$
CYG X-1(REF)
A-3
A-4 LED
A-4 MED
FLUX (PHOTONS/cm^2-sec-keV)
ENERGY (keV)
10^{-1}
10^{-2}
10^{-3}
10^{-4}
10^{-5}
10^0
10^1
10^2
10^3

Figure 18

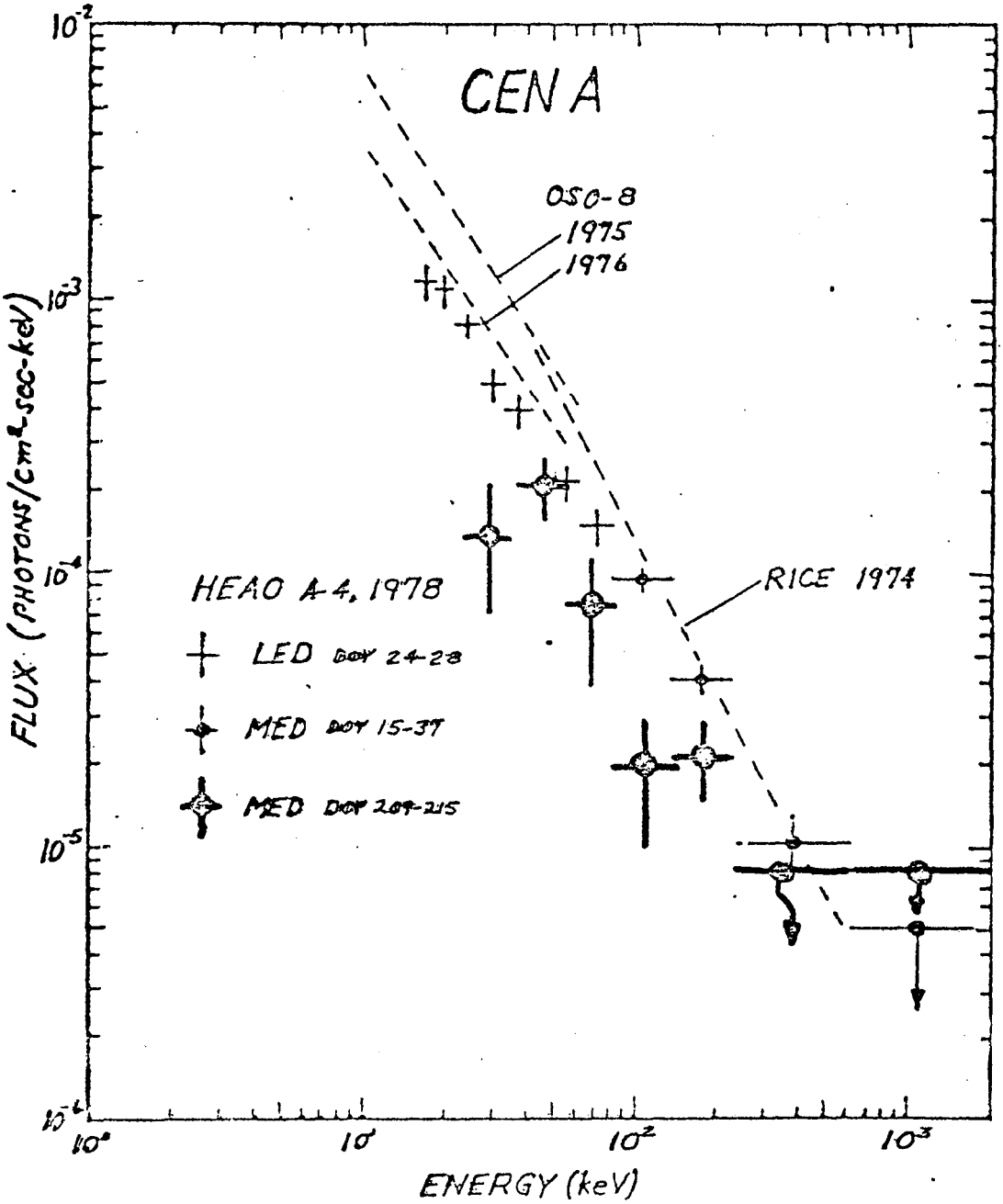
CEN A
OSO-8
1975
1976
HEAO A-4, 1978
LED DOY 24-28
MED DOY 15-37
MED DOY 209-215
RICE 1974
FLUX (PHOTONS/cm²-sec-keV)
ENERGY (keV)

Figure 19

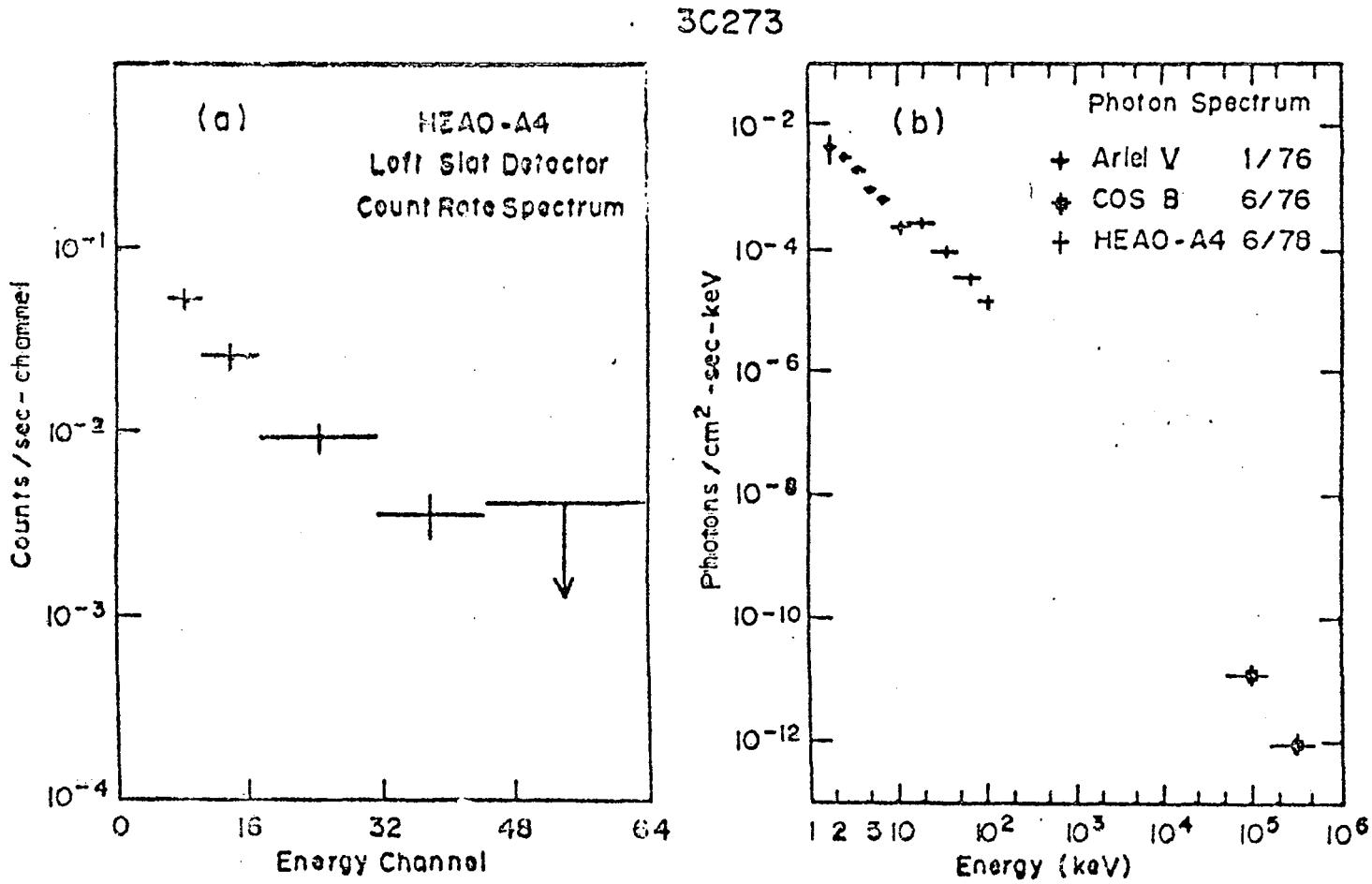
3C273
(a)
HEAO-A4
Low Slat Detector
Count Rate Spectrum
Counts / sec - channel
Energy Channel
(b)
Photon Spectrum
Ariel V 1/76
COS B 6/76
HEAO-A4 6/78
Photons / cm² - sec - keV
Energy (keV)

Figure 20

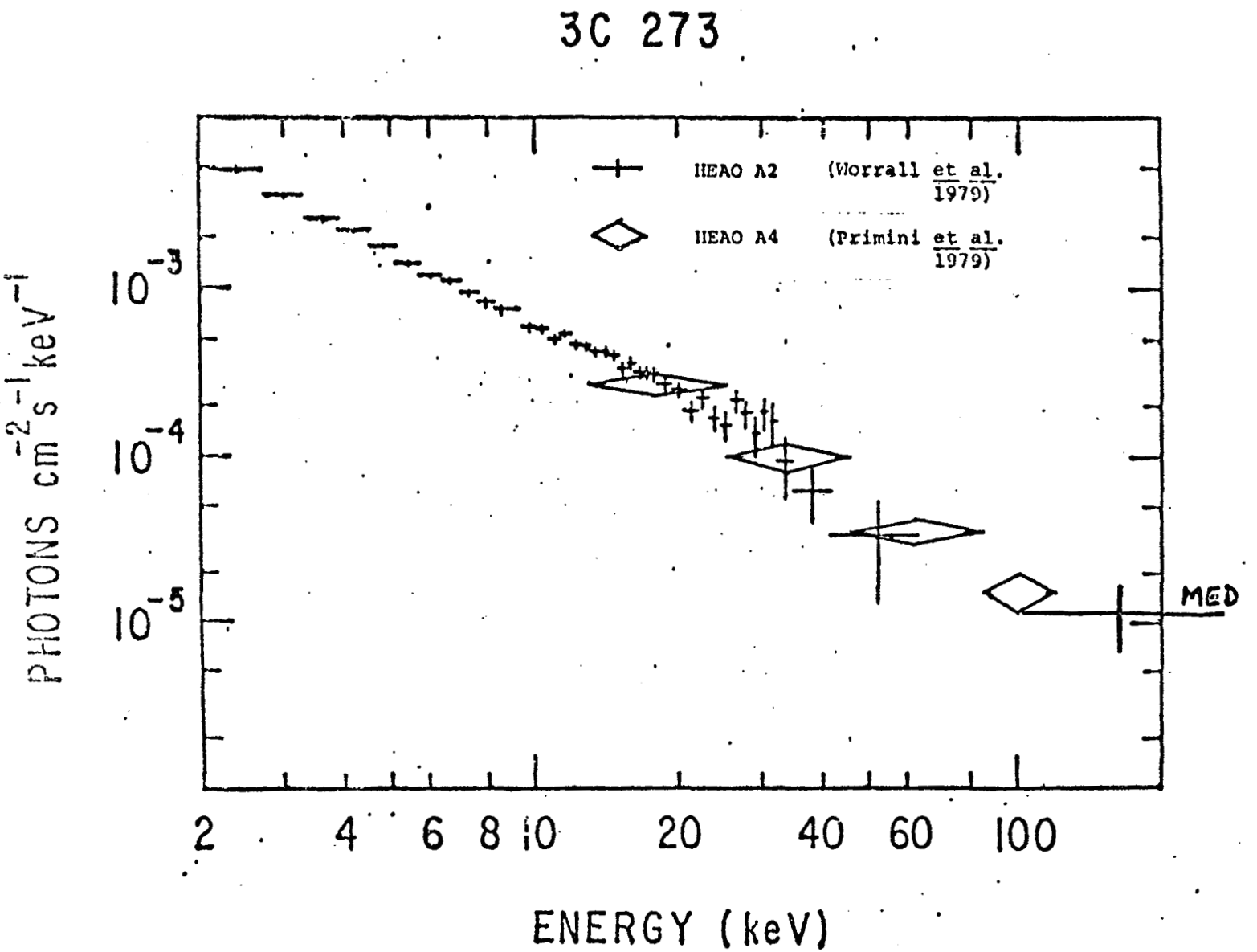
3C 273
HEAO A2 (Worrall et al. 1979)
HEAO A4 (Primini et al. 1979)
MED
PHOTONS cm^{-2}s^{-1}keV^{-1}
10^{-3}
10^{-4}
10^{-5}
2
4
6
8
10
20
40
60
100
ENERGY (keV)

Figure 21

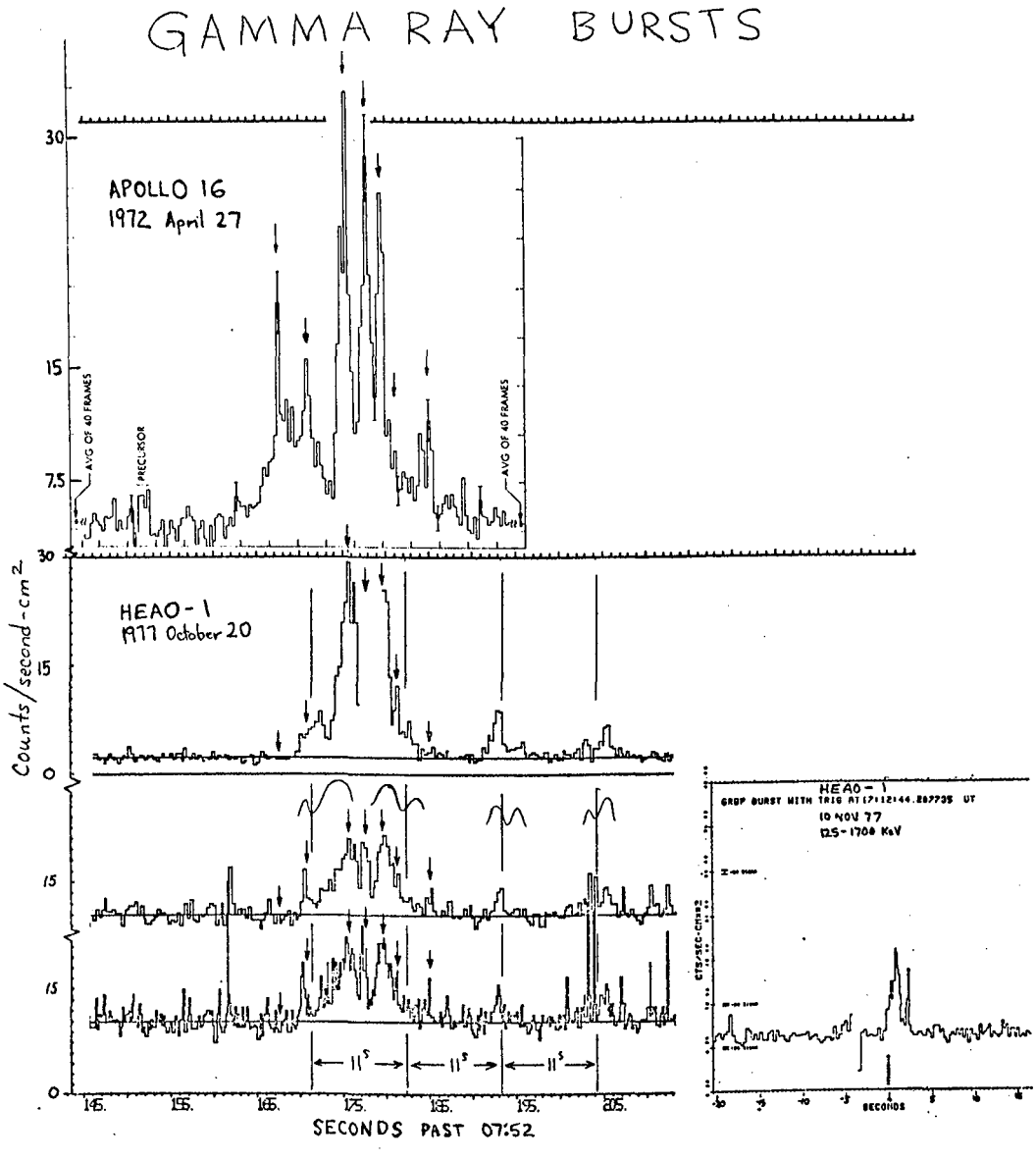
GAMMA RAY BURSTS
APOLLO 16
1972 April 27
AVG OF 40 FRAMES
PRECURSOR
AVG OF 40 FRAMES
HEAO-1
1977 October 20
Counts/second-cm²
11ˢ
11ˢ
11ˢ
SECONDS PAST 07:52
HEAO-1
10 NOV 77
SECONDS

Figure 22

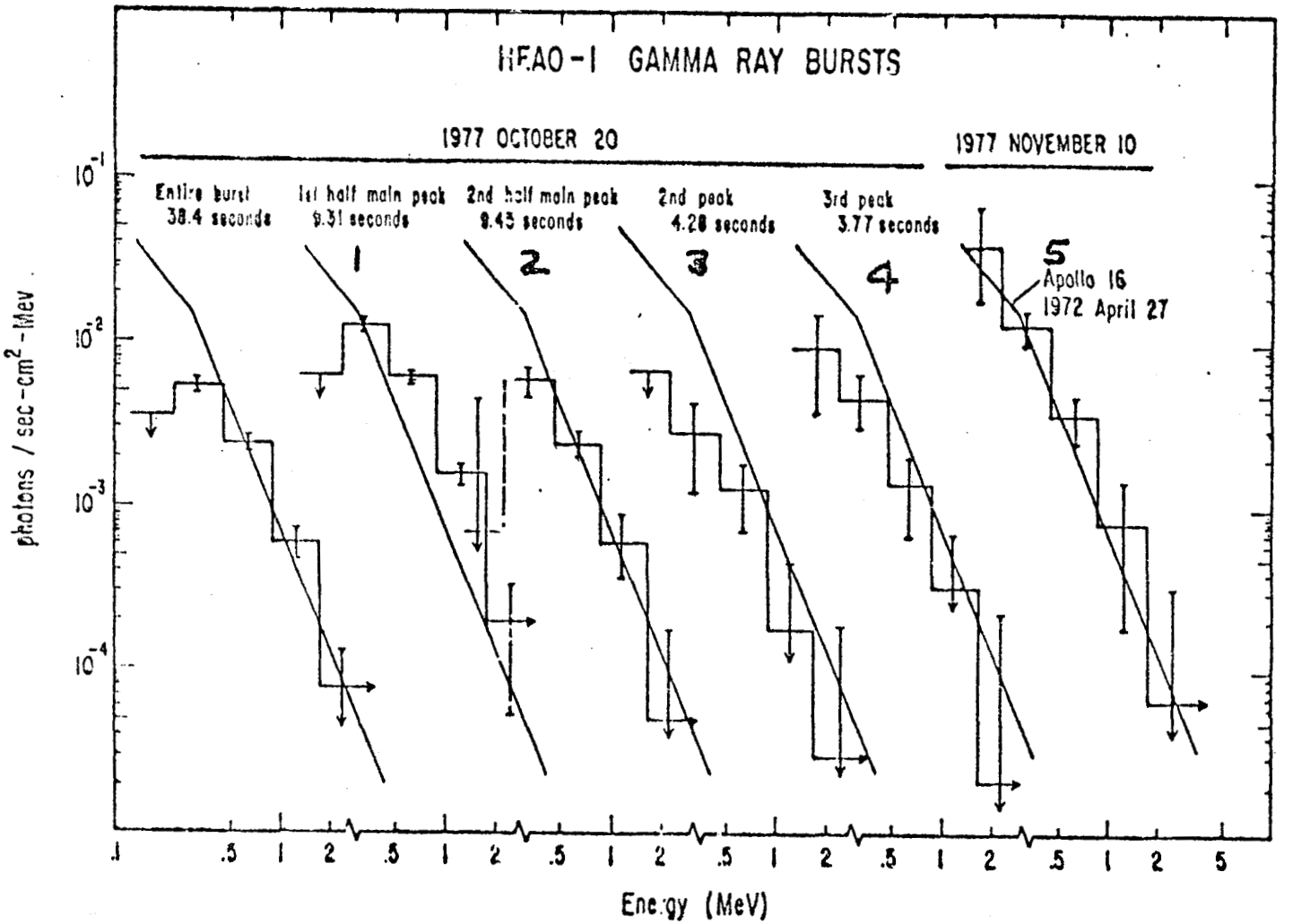
HEAO-1 GAMMA RAY BURSTS
1977 OCTOBER 20
1977 NOVEMBER 10
Entire burst
38.4 seconds
1st half main peak
9.31 seconds
2nd half main peak
9.43 seconds
2nd peak
4.28 seconds
3rd peak
3.77 seconds
1
2
3
4
5
Apollo 16
1972 April 27
photons / sec-cm^2-Mev
10^{-1}
10^{-2}
10^{-3}
10^{-4}
.1
.5
1
2
5
Energy (MeV)

Figure 23